THE JOURNAL OF PHYSICAL CHEMISTRY B

ARTICLE

pubs.acs.org/JPCB

Pump−Dump−Probe and Pump−Repump−Probe Ultrafast Spectroscopy Resolves Cross Section of an Early Ground State Intermediate and Stimulated Emission in the Photoreactions of the Pr Ground State of the Cyanobacterial Phytochrome Cph1

Ann E. Fitzpatrick, Craig N. Lincoln, Luuk J. G. W. van Wilderen, and Jasper J. van Thor*

Division of Molecular Biosciences, Imperial College London, South Kensington, SW7 2AZ

Supporting Information

ABSTRACT: The primary photoreactions of the red absorbing ground state (Pr) of the cyanobacterial phytochrome Cph1 from *Synechocystis* PCC 6803 involve C15═C16 *Z*−*E* photoisomerization of its phycocyanobilin chromophore. The first observable product intermediate in pump−probe measurements of the photocycle, "Lumi-R", is formed with picosecond kinetics and involves excited state decay reactions that have 3 and 14 ps time constants. Here, we have studied the photochemical formation of the Lumi-R intermediate using multipulse picosecond visible spectroscopy. Pump−dump−probe (PDP) and pump−repump−probe (PRP) experiments were carried out by employing two femtosecond visible pulses with 1, 14, and 160 ps delays, together with a broadband dispersive visible probe. The time delays between the two excitation pulses have been selected to allow interaction with the dominant (3 and 14 ps) kinetic phases of Lumi-R formation. The frequency dependence of the PDP and PRP amplitudes was investigated at 620, 640, 660, and 680 nm, covering excited state absorption (λ_{max} = 620 nm), ground state absorption (λ_{max} = 660 nm), and stimulated emission (λ_{max} = 680 nm) cross sections. Experimental double difference transient absorbance signals (ΔΔOD), from the PDP and PRP measurements, required corrections to remove contributions from ground state repumping. The sensitivity of the resulting ΔΔOD signals was systematically investigated for possible connectivity schemes and photochemical parameters. When applying a homogeneous (sequentially decaying) connectivity scheme in both the 3 and 14 ps kinetic phases, evidence for repumping of an intermediate that has an electronic ground state configuration (GSI) is taken from the dump-induced S1 formation with 620, 640, and 660 nm wavelengths and 1 and 14 ps repump delays. Evidence for repumping a GSI is also seen, for the same excitation wavelengths, when imposing a target connectivity scheme proposed in the literature for the 1 ps repump delay. In contrast, using a 680 nm dump pulse, ground state formation is observed for all models examined. The ΔΔOD signals were dominated by stimulated emission, at both 1 and 14 ps delays for the longer wavelength excitation. The GSI, which is revealed by the PRP measurements and not resolved from pump−probe measurements, is found to be directly formed from the excited state of Pr, and its formation is considered using heterogeneous, homogeneous, and target models to globally fit the data.

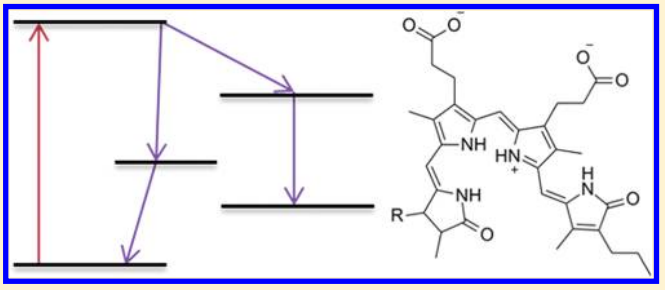

1. INTRODUCTION

Phytochromes are a family of light-sensitive proteins acting as photoreceptors for biological signaling, which usually have reversible red ("Pr") and far red ("Pfr") absorbing forms.[1−4] The cyanobacterial phytochrome Cph1 from *Synechocystis* PCC 6803 has spectroscopic transitions similar to those observed in plant phytochrome receptors, with the Pr state absorption maximum at 660 nm and the Pfr metastable intermediated maximum at 710 nm. The Pfr intermediate is long-lived with thermal reversion occurring on a second time scale.[5] Pfr can additionally be phototransformed by far red light back to the Pr ground state.[6,7]

Phytochromes are involved in many physiological roles such as seed germination, optimization of growth, and phototropism and have been found in plants, fungi, bacteria, and cyanobacteria.[1−4] The whole family appears to share common photophysical properties. It is widely accepted that the interconversion between the Pr and Pfr forms is triggered by a photoinduced *Z*−*E* and *E*−*Z* photoisomerization, respectively, around the C15═C16 double bond of the billin chromophore.[1,2] Additional structural rearrangements in the phycocyanobilin chromophore of Cph1, particularly at C5, during the photocycle have been implicated from NMR[8] and time-resolved infrared (TRIR) measurements.[6]

A variety of spectroscopic techniques have been used to study the phytochrome family to gain insight into the dynamics of the photoreactions.[1−15] Cph1 has been studied using several ultrafast spectroscopic techniques such as visible and infrared transient absorption (TA) spectroscopy[6,9,13,15] as well as by femtosecond

Received: July 4, 2011
Revised: November 18, 2011
Published: November 19, 2011

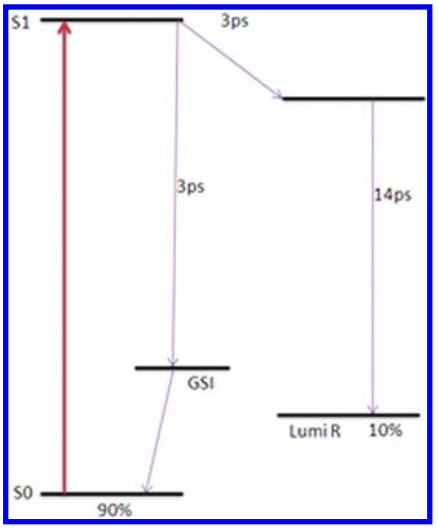

Figure 1. Proposed reaction model and time constants used to describe the photodynamics of the Pr state of Cph1 suggested by ref 15. The red arrow indicates excitation by absorption of a photon, and gray arrows indicate suggested decay pathways. The model includes a ground state intermediate (GSI) and contains a mixture of parallel and sequential exponential decays. The quantum yield is also indicated.

stimulated Raman spectroscopy (FSRS).[10] A visible pump−probe spectroscopy study modeled the ultrafast dynamics of the Pr state of Cph1 by employing a distribution of rate constants centered at 16 ps or a sum of two time constants between 11 and 15 ps and 48−97 ps depending on excitation wavelength.[13] Using these pump−probe TA measurements, assignments were made for the ground state bleach (GSB) at 660 nm, excited state absorption (ESA) at 600−640 nm, and stimulated emission (SE) at 680 nm, with SE and ESA overlapping with GSB.[13] It was noted that the Lumi-R minus Pr difference spectrum at 300 ps had decayed to very small amplitude, with a negative feature at 665 nm and weak product absorption at 700 nm, indicating that Lumi-R has an absorption spectrum that is strongly overlapping with Pr.[13] Considering the approximately 10% quantum yield for Lumi-R formation, its spectrum is characterized by a reduced absorption cross section and a small red-shift relative to Pr.[13] Singular value decomposition (SVD) of TA infrared spectroscopy measurements distinguished three time components (3, 14, and 134 ps) to describe the dynamics of Lumi-R formation.[6] The spectral differences in the mid-infrared region for all three phases were shown to be highly similar and dominated by S1 decay, showing strongly reduced absorption cross section, particularly for C═C stretching modes.[6] Without further information regarding connectivity of the intermediates, the data were globally fitted using a heterogeneous model that used the sum of three exponentials, decaying in parallel. In addition to the heterogeneous model, calculated using a sum of weighted exponentials, a homogeneous and target model are also applied to the data to assess their suitability in describing the Pr photoreaction. A homogeneous model employs coupled differential equations to resolve intermediates, and the target model is a mixture of both homogeneous and heterogeneous decay pathways and is displayed pictorially in Figure 1.

A previous PDP and PRP study of Cph1 with TRIR revealed formation of an S1 state with a repump pulse at 640 nm and 14 ps delay, that is spectrally distinct from S1 observed after pumping of Pr.[15] This was taken as evidence for a transient population of a GSI at 14 ps in the pathway of Lumi-R formation, which was the motivation for the target model applied in this work[15] (Figure 1). Ultrafast vibrational FSRS measurements of the Pr state of Cph1 were interpreted with a specific target model,[10] involving an ultrafast excited intermediate formed in ∼500 fs, followed by a branching to reform the ground state with a 3 ps time constant (with 85% quantum yield) and Lumi-R being formed in 30 ps by excited state decay from Lumi-R*.[10] After subtractions and scaling of FSRS signals, intensity at 1629 cm^{-1}, assigned to delocalized modes comprising the C15═C16 and the C17═C18 bonds, was proposed to serve as a criterion of ground state population, from which a ground state recovery of 85% with 150 fs and 3 ps time constants was derived.[10] The assignment made[10] for the 1629 cm^{-1} mode however assumed a ZZZasa configuration in the Pr state, whereas more recently it was shown that for the ZZZssa conformation the assignment is made to the C4═C5 mode.[6] An additional argument that the fluorescence quantum yield of 0.5%[9,11] would not support formation of the Lumi-R ground state on this time scale did not take into account the amplitude and spectral differences that were determined from TRIR.[6] Specifically, the spectra associated with 3 and 14 ps components are very similar in the 1450−1750 cm^{-1} region, and global analysis provided 38% and 52% amplitude for the components, respectively. Therefore, information from FSRS, TRIR, or vis−vis pump−probe measurements cannot directly provide conclusive evidence for the connectivity with regard to which phase is productive in Lumi-R formation. In contrast, additional information can be obtained from multipulse measurements where a dump or repump pulse selectively manipulates the evolving populations after initial photoexcitation, which can have ground or excited state configurations.[15−24]

Ultrafast TA spectroscopy can probe both coherent and incoherent reaction phases. At room temperature in the condensed phase, the electronic decoherence time is typically a fast femtosecond process.[25] Multiple interactions taking place within the decoherence time give rise to nonlinear phenomena, whether these result from multiple optical pulses or within the envelope of a single intense pulse. For instance, Rabi cycling is a coherent process that occurs at intense electrical field strengths within the dephasing time. After decoherence, the optically excited system retains the population differences for the duration of the population decay time constant. PDP experiments take place in this regime to cause population inversion by incoherent manipulation.

Multipulse spectroscopy has been applied to proteins and chromophores since 1997 when this technique was originally used to investigate intermediates in the photoreactions of bacteriorhodopsin.[16] In this initial experiment a GSI, invisible in pump−probe experiments, was observed for the first time. Applying a dump pulse to an excited bacteriorhodopsin sample caused a large instantaneous population transfer toward the ground state. The stimulated emission from the sample was measured to monitor the reaction dynamics, revealing a GSI.[16] The use of a dump pulse to instantly remove population from excited and intermediate states is one way that reaction dynamics have been successfully manipulated using multipulse spectroscopy, revealing connectivity schemes and spectroscopically invisible states.

Instead of returning population to the ground state, the interacting pulse can promote the system of interest to a higher excited state. A heterogeneous decay pathway was discovered in bacteriorhodopsin the first time this technique was performed in 2001.[21] Relaxation of the repumped population to the ground state was monitored by measuring the stimulated emission of the S1 state. When the S1 state in bacteriorhodopsin was repumped,

the recovery time and subsequent decay of the stimulated emission from the S1 state changed with the delay between the pump and repump pulses. The alteration in dynamics reveals a separate decay pathway from the Sn state to the ground state that is not populated during pump−probe experiments.[21]

Only a small number of PDP and PRP experiments have been carried out to date,[15−24,26] with each experiment showing the power of multipulse spectroscopy to disentangle spectrally overlapping states and connectivity schemes. The systems studied with multipulse techniques include photoactive yellow protein,[19,20] Green Fluorescent Protein (GFP),[17,26] retinal,[23] peridinin,[22] and carotenoids, as well as bacteriorhodopsin[16,21] discussed above and Cph1 using the infrared.[15] Typical dynamics that can be monitored by the PDP/PRP technique are on the order of picoseconds making Cph1 a suitable system to study with visible PDP/PRP spectroscopies as it has displayed dynamics on this time scale.[6,10,13]

In materials such as the GFP[17,26] and peridinin,[22] GSIs present in the photoreactions decay faster than they are populated. As a result, a detectable population does not accumulate during the photocycle, and the state is invisible in pump−probe experiments. The dump-induced population transfer increases the instantaneous population of the GSI to resolvable levels, allowing it to be detected and its dynamics monitored.[17,22] In the photoactive yellow protein chromophore, a GSI has also been resolved by manipulating the evolving states to produce a detectable population in the GSI after the dump pulse, evident by ESA and SE signal reduction, indicating the transfer of population.[20]

The large population transfers instigated by PDP and PRP can permit spectrally similar states to be resolved. For the retinal chromophore of proteorhodopsin, spectral similarity between the GSI and SE renders the GSI invisible in pump−probe experiments. The large instantaneous population induced by a dump pulse is required to detect the GSI as a separate state.[23] A similar situation is found in the carotenoid β-carotene, where the broad ESA was revealed to be heterogeneous by the application of a dump pulse. It was observed that the population transfer, caused by the pulse, only reduced the ESA band over part of the wavelength range indicating that two excited states were populated.[18]

The above-mentioned examples show that PDP and PRP spectroscopy has been able to reveal intermediates that are not detectable from conventional pump−probe spectroscopies for one of two commonly encountered reasons. Either an intermediate is hidden because it decays faster than it is formed or it has reduced cross section or spectrally closely overlaps with the ground state or an intermediate. An example of the second possibility, we believe, is a ground state intermediate in the photocycle of Cph1 revealed in this work.

Here, we present multiple single-wavelength PDP/PRP measurements of the Pr state of Cph1 and apply the analysis described in eq 4 to resolve the wavelength dependence of the dump and repump excitations. The results demonstrate that the SE cross section for the S1 state increases at longer wave lengths and reveals the presence of a short lived GSI, produced by either the 3 ps component or the 3 and 14 ps components depending on which connectivity scheme correctly describes the Cph1 Pr photocycle.

2. METHODS

2.1. Sample Preparation and Conditions. The Cph1Δ2 fragment of *Synechocystis* PCC 6803 Cph1 was coexpressed in *Escherichia coli* with heme oxygenase and billin reductase genes from *Synechocystis* and purified using affinity and size exclusion fast protein liquid chromatography as described previously.[8] The purified protein was concentrated to an optical density of 0.3 for a 100 μm path length at 660 nm, the peak of the Pr ground state absorbance. The buffer solution used was 5 mM tris, 50 mM NaCl, and pH 7.8 at room temperature.

The protein sample was placed between fused silica windows with a 100 μm Teflon spacer, in a flow cell (Harrick scientific products). In addition to flowing the sample, which replaces the sample on a second to minute time scale, the sample cell was also rapidly translated to ensure a fresh sample in the laser interaction region on a shot-to-shot basis as previously described.[8,15] Continuous illumination of the sample with a far red LED (LedEngin, λ_{max} = 735 nm, FWHM = 30 nm, 310 mW) was employed to ensure that any Pfr formed was converted back to the Pr ground state during data acquisition. The steady state absorption spectrum of the sample was taken directly after every measurement to verify that no Pfr was built up under experimental conditions that combine both far-red background illumination and visible laser beams for pump−probe and PDP/PRP measurements, as previously described.[6,14] The −50 ps spectrum is used as background and shows a small contribution from a millisecond component, characterized by an amplitude which corresponds to less than 1% of the total sample absorbance and less than 10% of the transient signal present at (positive) picosecond delays.

2.2. Visible Pump−Probe, PDP, and PRP Spectroscopy. Time-resolved visible TA measurements of the Pr state were made with femtosecond optical excitation. The excitation of Pr was performed at four different wavelengths resonant with the Pr ground state at the blue, center, and red edge at 620, 640, 660, and 680 nm. The power density was adjusted according to the wavelength dependence of the ground state cross section such that the photolyzed fraction was approximately 10%, to avoid nonlinear transitions and to optimize the signal-to-noise ratio for the measurements. Absorption changes were monitored using delays between 400 fs and 2 ns from 450 to 700 nm.

The excitation pulses were generated using an optical parametric amplifier (OPA, Spectra Physics, OPA-800C) pumped with the fundamental (800 nm) output of a 1 kHz titanium-sapphire laser (Hurricane, Spectra Physics). Pump, dump, and repump excitation at 620, 640, 660, and 680 nm wavelengths were generated from sum frequency mixing from the OPA with ≈90 fs (FWHM = 15 nm) pulse duration (measured using an autocorrelator, Spectra Physics, SSA). The output from the OPA was split to create two beams. In the sample plane, the diameter of the two excitation pulses was 145 and 195 μm with pulse energies of ≈100 and ≈120 nJ depending on wavelength. The pulse energy ensured the experiment was conducted with fractional photolysis less than 10%. Delay lines (Newport, high-performance linear stage, 0.1 μm resolution, M-IMS400CCHA) in the optical setup allowed programmable time delays between the pump and the probe beams. The time delay between the pump and dump pulses was fixed with a manual translation stage (ThorLabs) at 1, 14, or 160 ps, which was used for all of the excitation wavelengths. The probe pulse was produced using a fraction of the fundamental output, which was focused into a 1 mm thick sapphire plate to generate a white light continuum that spanned from 450 up to 750 nm, which was attenuated to 6 nJ energy and focused to a 75 μm diameter spot. Detection was done dispersively from λ = 500 to 750 nm at 1 kHz repetition rate and intensity. Spectral fluctuations were reduced by referencing each pulse by using a second synchronized detector.

Pump−probe measurements of Cph1 were obtained as shown in eq 1 by subtracting the spectrum collected from an unpumped measurement.

$$\Delta\mathrm{OD}(\lambda, t) = \mathrm{Pump(on)}(\lambda, t) - \mathrm{Pump(off)}(\lambda) \quad (1)$$

where t is the time delay between pump and probe. Additionally, one or more negative pump time measurements, typically at −50 ps, are acquired and used for additional correction.

Pump−probe and PDP/PRP data were collected using two optical choppers (Thorlabs, MC1000A) to yield a pump pulse repetition frequency of 500 Hz and dump/repump pulse repetition frequency of 250 Hz. This permitted all combinations (pump−dump/repump−probe, pump−probe, dump/repump−probe, and probe only) of pulses to be collected. The detection scheme employed here uses 1024 channels for a 300 nm spectral window with dispersive detection such that global fitting of spectral differences supports the observed kinetics of many measurements.

Most multipulse spectroscopy carried out to date employs different wavelengths for the visible excitation pulses in the PDP or PRP pulse sequence.[16−24] Typically, the dump or repump excitation parameters are chosen to minimize resonance with the ground state and to maximize resonance with reaction intermediates. Data collection of the PDP/PRP signal arising from the double excitation ultimately gives ΔΔOD signals which are obtained by subtraction as follows

$$\Delta\Delta\mathrm{OD}(\lambda, t, \tau) = \mathrm{PDP}(\lambda, t, \tau) - \mathrm{PP}(\lambda, t) \quad (2)$$

where λ and t represent the wavelength and delay of the probe and τ the dump or repump pulse delay. In this approach, the TA amplitude from the dump excitation of the ground state is neglected when there is a reduced ground state absorbance cross section. The dump or repump dynamics are obtained by scanning either t or τ in eq 1 to provide either "pump−dump−probe dynamics" or "dump action trace".[22] However, pump−probe amplitudes from the dump or repump excitation resulting from resonance with the ground state are not usually negligible. A first-order approach would subtract the dump signal as follows.

$$\Delta\Delta\mathrm{OD}(\lambda_1, \lambda_2, t_1, t_2) = \mathrm{PDP}(\lambda_1, \lambda_2, t_1, t_2) - \mathrm{PP}(\lambda_1, t_1) - \mathrm{DP}(\lambda_2, t_2) \quad (3)$$

where t_1 and t_2 are the delays between the visible pulses and the probe, and the difference signals for the three-pulse measurement (PDP) and both two-pulse measurements (PP = pump−probe, DP = dump− or repump−probe) are the pump−probe signals with excitation at wavelengths λ_1 and λ_2.[15,27] Equation 3 is valid in the limit where excitation triggers negligible transient populations, such that the DP amplitude is equal to its contribution within the PDP signal. However, for TA spectroscopy conducted under excitation conditions leading to photolysis fractions in the 0.01−0.1 range, eq 3 is not valid. Furthermore, linearly polarized visible pulses selectively photolyze populations within the isotropically oriented ensemble. Therefore, the residual ground state population is partially oriented, and population decay following the pump excitation proceeds independent of this orientation. It was previously shown that calculation may correct for the orientation and population distribution as follows[27]

$$\Delta\Delta\mathrm{OD}(\lambda, t_{\mathrm{delay}}, t_{\mathrm{pr}}) = \mathrm{PDP}(\lambda, t_{\mathrm{delay}}, t_{\mathrm{pr}}) - \mathrm{PP}(\lambda, t_{\mathrm{pr}}) - \alpha(t_{\mathrm{delay}})\mathrm{DP}(\lambda, t_{\mathrm{pr}}) \quad (4)$$

where PDP is the pump−dump/repump−probe signal; PP and DP are the pump−probe and dump/repump−probe TA signals, respectively; and α is a scaling factor to be applied to the dump/repump signal to account for the power and polarization dependence of the photolyzed fraction, which may be evaluated from calculations that apply photoselection theory.[27] In the notation used in eq 4, PP and DP are two pump−probe experiments with the probe timings for DP shifted by the delay between the two excitation pulses. Further corrections take into account the explicit Gaussian or multimode beam shape and diameters, to estimate the photolyzed fractions.[27] It was previously shown that eq 4 should be used to provide the best possible estimate of the ΔΔOD signal either for single color or dual color PDP/PRP experiments.[27]

Equation 4 yields the ΔΔOD TA signals that correspond to the dump or repump excitation interacting exclusively with the intermediate states created by the pump. In this approach, it is essential that values for the scaling factor α are taken from careful measurements of power density and fitted time constants from pump−probe data. In addition, scaling is sensitive to connectivity models that are applied to the pump−probe TA data. Methods for deriving these parameters have been developed and reviewed in detail previously.[27,28] Briefly, the ensemble averaged photolysis fraction for each population is calculated from carefully measured power density profiles and the relevant cross sections. The ensemble averaged photolyzed fraction for the reduced (i.e., previously excited) ground state population, $\langle n_2 \rangle$, is divided by the ensemble averaged photolyzed fraction for the complete ground state $\langle n_1 \rangle$ that arises from single pulse excitation, as shown in eq 5. This scaling factor α is subsequently used in eq 4 to obtain the corrected double difference signals.

$$\alpha = \frac{\langle n_2 \rangle}{\langle n_1 \rangle} \quad (5)$$

The fraction of an ensemble of randomly oriented molecules that are excited by the application of a laser pulse depends on the molecular properties of the particles and parameters of the excitation pulse. Important parameters include the absorption cross section, photon flux, and orientation of the transition dipole relative to polarization of the incoming laser pulse. Because of the dependence on molecular orientation relative to the laser polarization, photoselection by the pump pulse produces an anisotropic orientation, which is also time dependent and will evolve as the photocycle progresses. This anisotropy in the orientation requires an additional calculation, to assess the time-dependent recovered ground state population, to accurately determine the ensemble averaged photolyzed fraction induced by the dump or repump pulse. Explicit discussion of the photoselection theory needed for these calculations can be found in refs 27 and 28.

3. RESULTS

3.1. Pump−Probe Transient Absorption Spectroscopy. Figure 2 shows a 2D plot of the pump−probe data for excitation at 640 nm as well as (globally fitted) time traces for selected wavelengths overlaid with the raw data to indicate the fit quality across the wavelength range measured. The pump−probe signals collected for all excitation wavelengths employed (620, 640, 660, and 680 nm) display comparable spectral shape and decay dynamics as can be seen in the Supporting Information

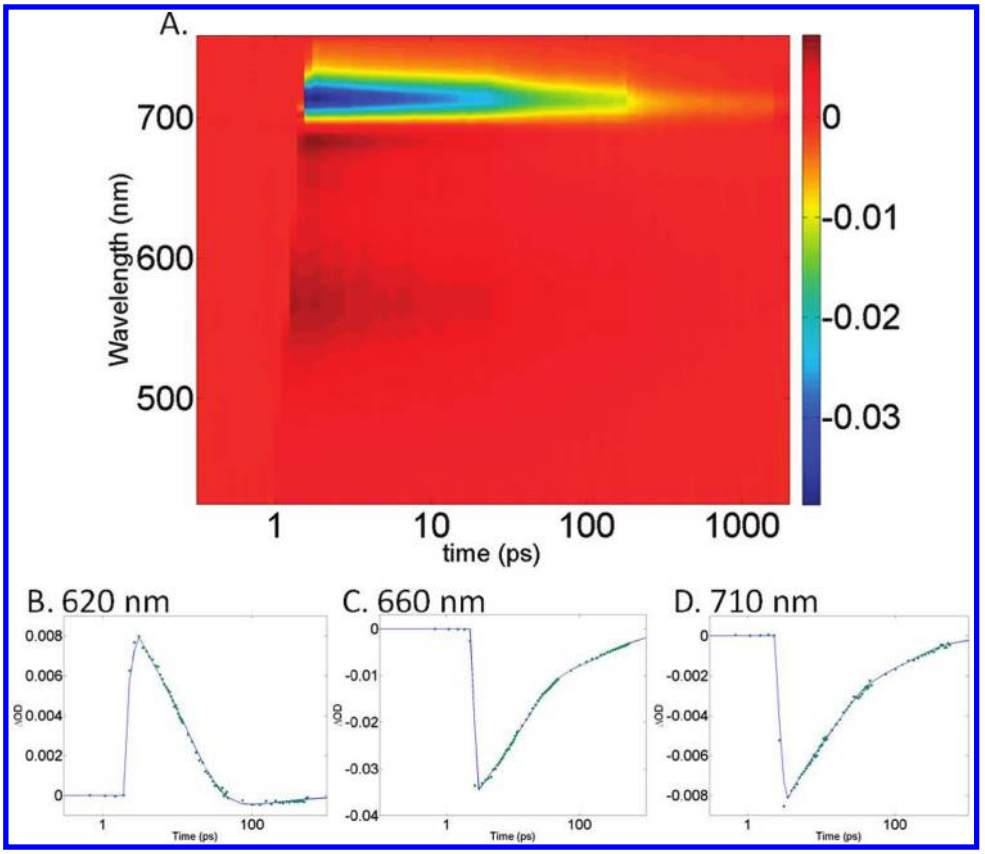

Figure 2. TA results of Pr excited with 640 nm. Panel A shows a 2D plot to give an overview of the spectral and temporal shape of the background corrected ΔOD signal. Panels B, C, and D globally fitted time traces for wavelengths as indicated in the figure (blue line), overlaid with the measured signal (green dots).

(Figure S1) where spectra for selected time delays are shown for all excitation wavelengths. At early delay times, the difference spectrum exhibits a large negative feature around 670 nm and a positive feature stretching from 640 to 450 nm. The difference spectra decay without significant change to the spectral shape, although the ESA at 620 nm decays faster than at 500 nm. The TA difference spectrum is made up of a superposition of negative GSB and SE and positive ESA. SE dominates the signal at long wavelengths (>700 nm), and ESA partially cancels the short-wavelength (≈640 nm) portion of the GSB. Other contributing intermediates cannot be easily identified. For data between 600 and 700 nm the assignments are broadly in agreement with those previously reported from single wavelength pump−probe measurements.[13] ESA present between 450 and 550 nm are reported here for the first time.

At long delays (2 ns) an induced absorption feature appears at 670 nm, indicating the formation of the product intermediate Lumi-R. The maximum of the GSB and SE features shifts by 5 nm from 670 nm toward shorter wavelengths at long times once the excited state population has been reduced. After 200 ps, the wavelength of the GSB feature coincides with the maximum of the steady state absorption of the Pr ground state.

Singular Value Decomposition (SVD) and global analysis[27,29] of the data were carried out using the population dynamics modeling toolbox software developed by van Wilderen et al.[27] Homogeneous (amplitudes sequentially decaying) and heterogeneous (amplitudes decaying in parallel) decay pathways were used to model the data as well as a target model, shown in Figure 1. All three models applied produced good fit results with three time constants and a long-lived component of 500−800 ps in the SVD analysis. SVD results were obtained from fitting the left singular vectors for the first three significant components after multiplication with their singular values. The long-lived or 500 ps component from the fitting represents the formation of the Lumi-R product. Species associated spectra for the homogeneous model at all excitation wavelengths are shown in Figure 3, and species associated spectra for the heterogeneous and target models are shown in the Supporting Information (Figures S2 and S3). The resulting time constants from the global analysis and SVD are summarized in Table 1 for the application of the homogeneous model. Similar time constants are obtained for the heterogeneous and target models, the results for global and SVD analysis imposing these models is presented in the Supporting Information (Tables S1 and S2).

The time constants calculated from the global analysis are similar for all applied models and excitation wavelengths. The time constants calculated from the data are consistent with those already reported in the literature,[6,10,13] except for a 500 fs component reported from FSRS which is not resolved in our experiment.[10] No significant spectral or kinetic differences were evident between the experiments conducted at different excitation wavelengths, in contrast to previously reported pump−probe measurements of Cph1.[13] Specifically, within the instrument response reported here, there is no direct evidence for the creation of hot intermediates with excitation in the blue edge of the ground state

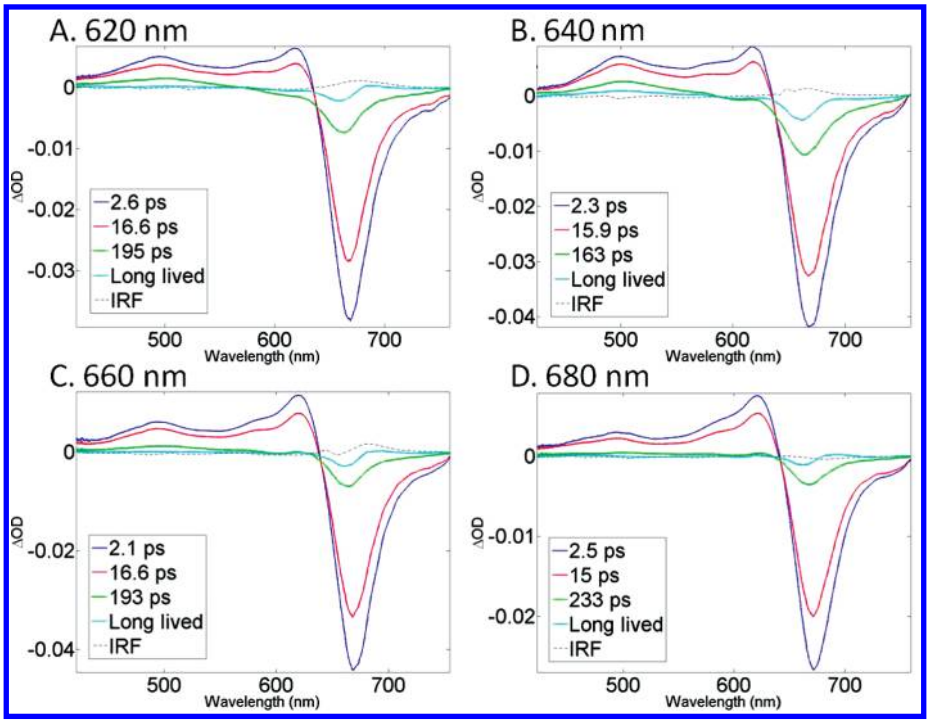

Figure 3. Species associated difference spectra of the dynamics of the Pr state of Cph1 after photoexcitation. Spectra are obtained from global fitting using a homogeneous decay pathway for different excitation wavelengths as indicated in the figure. Associated time constants, τ_i, are shown in the legend in picoseconds, and IRF is the modelled instrument response function.

Table 1. Results of Pump−Probe Analysis with the Homogeneous Model[a]

λ (nm)	τ_1 (ps)	τ_2 (ps)	τ_3 (ps)
620	2.57 ± 0.01	16.56 ± 0.02	194.61 ± 5.69
640	2.27 ± 0.01	15.91 ± 0.25	163.13 ± 10.62
660	2.11 ± 0.01	16.60 ± 0.21	192.66 ± 13.11
680	2.50 ± 0.09	14.96 ± 0.01	233.33 ± 8.99

λ (nm)	τ_1 (ps)	τ_2 (ps)	τ_3 (ps)	τ_4 (ps)
620	2.68 ± 0.01	14.36 ± 0.01	160.59 ± 11.84	long lived
640	2.61 ± 0.05	12.19 ± 1.03	81.96 ± 10.95	602.66 ± 82.09
660	2.36 ± 0.47	12.82 ± 1.01	84.80 ± 23.50	773.21 ± 261.42
680	2.89 ± 0.08	14.45 ± 0.01	229.98 ± 57.47	long lived

[a] Time constants, τ_i, from global analysis (top) and SVD (bottom) of Cph1 pump−probe data using a homogeneous model. Global analysis was performed on complete, background corrected data sets with excitation at 620, 640, 660, and 680 nm up to 2 ns delay. SVD results were from simultaneous fitting of left singular vectors for the first three significant components, scaled with the singular values for the decomposition of the same data sets. The *s* values for the different excitation wavelengths are: for 620 nm (1.07, 0.106, 0.0180), for 640 nm (1.32, 0.112, 0.0209), for 660 nm (1.28, 0.843, 0.0246), for 680 nm (0.764, 0.0387, 0.0189). The error given is the standard deviation.

transition at 620 nm, as previously put forward on the basis of single-wavelength pump−probe measurements of Cph1-Pr.[13]

3.2. Evaluation of Model Dependence for MultiPulse Spectroscopy Data Corrections. Equation 4 provides a realistic estimate of the background corrected ΔΔOD signal relating to the population transfer of short-lived intermediates exclusively. The principle requirements include careful evaluation of quantum yield and power density dependence. Furthermore, a dependence on the reaction model applied results from the differences in the ground state recovery fraction that is included in the calculation (eq 5). Equations 5−8 describe the procedure and elements required to calculate α, and these factors are discussed in more detail below. Here, we consider the model dependence and resulting ground state recovery for dump/repump times (1, 14, and 160 ps), in addition to an estimate taken directly from the TA value near the GSB (eq 6).

$$1 - \beta(t) \approx \frac{\Delta\mathrm{OD}(t = 0) - \Delta\mathrm{OD}(t = d)}{\Delta\mathrm{OD}(t = 0)} \qquad (6)$$

where $1 - \beta(t)$ is the estimated recovered ground state fraction normalized to the initially excited state population; $\Delta\mathrm{OD}(t = 0)$ is the amplitude of the GSB, at 660 nm, resulting from the pump excitation; and $\Delta\mathrm{OD}(t = d)$ is the amplitude of the ground state bleach, at 660 nm, at the time delay d between the two excitation pulses. In these experiments, three time delays (d = 1, 14, or 160 ps) are used. Equation 6 provides an estimate of the ground state recovery by neglecting signal from ground state absorption, ESA, or SE and from intermediates. The Pr cross section appears to be higher than that of the intermediates, leading to Pr features dominating the spectra (Figure 3). The estimate from eq 6 is a starting point to begin to differentiate between the assumptions underlying each model shown. Table 2 lists the recovered ground state estimates for the different models and time delays.

3.3. Fractional Photolysis. The estimated fraction of molecules that is photolyzed by the excitation pulse can be calculated using photoselection theory[27,28] and established from the amplitude of the GSB using eq 7 for low levels of photolysis.

$$\langle n_{\mathrm{exp}} \rangle \approx \frac{\Delta\mathrm{OD}(t = 0)}{\mathrm{OD}} \qquad (7)$$

Table 2. Ground State Recovery Fractions[a]

model	1 ps recovered fraction	14 ps recovered fraction	160 ps recovered fraction
homogeneous	2.4×10^{-5}	0.024	0.59
heterogeneous	0.13	0.64	0.9
target	0.026	0.74	0.9
$1 - \beta(t)$	0.07	0.47	0.87

[a] Recovered Pr ground state estimates for delays of 1, 14, and 160 ps after initial laser excitation, imposing the homogeneous, heterogeneous, and target decay pathways (time constants taken from ref 6 or as shown in Figure 1) also estimated directly from the amplitude at 660 nm of the background corrected data using eq 6.

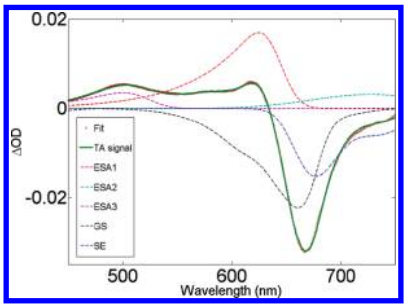

Figure 4. Spectral deconvolution of the instantaneous pump−probe difference spectrum with excitation at 640 nm. The signal is fitted using the measured Pr steady state spectra and fluorescent spectra to represent the GSB and SE components, respectively. Three EMG functions are applied to model ESA; all components shown on the graph are labeled in the legend. The fluorescent spectrum was taken from ref 30.

where $\langle n_{exp} \rangle$ is the experimentally calculated photolyzed fraction; $\Delta OD(t = 0)$ is the value of the GSB at 660 nm for $t = 0$; and OD is the steady state optical density of the Pr state at 660 nm. The amplitude of the TA signal at 660 nm has contributions from the ESA, GSB, and SE. To be able to accurately estimate the photolyzed fraction, from the instantaneous signal at 660 nm amplitude, the component of the signal relating to the GSB was extracted. An example of the signal fit and the constitute parts is shown in Figure 4. Three exponentially modified Gaussian (EMG) functions (eq 8) are used to model the excited state part of the TA signal; the steady state absorption of Pr is used to model the ground state contribution; and fluorescent spectra taken from ref 30 are used to model the SE.

A fit of the instantaneous signal using two EMG functions to model the ESA resulted in an unrealistic broad ESA feature stretching from 550 to 700 nm which was therefore rejected.

$$\frac{1}{\tau\sigma(2\pi)^{1/2}} \int_0^t e^{(-(t - t_g - t')^2/2\sigma^2)} . e^{(-t'/\tau)} dt' \qquad (8)$$

The results from these two methods of determining the photolyzed fractions are summarized in Table 3.

When calculating the photolyzed fraction using photoselection theory,[27,28] only the ground state cross section is taken into account, and unity quantum yield is assumed. Table 3 shows that the experimental amplitude is between 0.18 and 0.56 of the theoretical value. Coherent multiphoton absorption and optical nutation may be neglected at the experimental pulse length and peak power. Multiphoton transitions should not contribute at fractional photolysis levels below 10%, and these results are therefore strongly indicative of ultrafast internal conversion reactions occurring within the instrument response. Indeed, FSRS experiments resolved 500 fs dynamics assigned to ground state recovery.[10] Table 3 shows a systematic difference in the estimate for the quantum yield when either the pump or the dump/repump is used in isolation. As no significant wavelength dependence is demonstrated, the differences are likely to result from pointing and overlap variations between the two beams or from experimental errors in power density determination.

3.4. Photolyzed Fraction Corrections for Optically Thick Samples. The photolyzed fraction depends on the photon flux through the sample. In optically thick samples with a certain incident flux, the photolyzed fraction will decrease with depth. The transmitted intensity changes as a function of sample depth, as in eq 9.

$$J(z) = J_0 10^{-dz/z_0} \qquad (9)$$

where J_0 is the intensity at the front face of the sample; d is the sample absorbance; z_0 is the sample thickness; and z is the depth of the sample. Equation 9 can be used to calculate the intensity or photon flux through the sample depth, provided that the number of molecules exceeds the number of photons in the interaction region. The adjusted intensity is used to calculate the photolyzed fraction as a function of depth.[27]

For excitation at 640 nm, the photolyzed fraction calculated using the photo flux at the front face of the sample, under the conditions used, is 13.9%, whereas the depth average photolyzed fraction of the sample is 10.8%. Regardless of the difference, the resulting changes for the photolyzed fractions $\langle n_1 \rangle$ and $\langle n_2 \rangle$ from eq 3 have a negligible effect on the scaling factor, α. Therefore, depth averaging can be neglected under the conditions used.

3.5. Pump−Dump/Repump−Probe Scaling Factors. The scaling factor, α, for the different excitation wavelengths and different connectivity schemes obtained from eq 5 are given in Tables 4−6 separately for the delay times (1, 14, and 160 ps). Values are presented for all three models and are compared to the estimated scaling factors that arise from examining the instantaneous GSB signal using eq 6.

For a 1 ps delay, there are negligible differences between the models applied to estimate the scaling factor α since little population decay has occurred at that time (Table 4). The differences were more apparent for the 14 ps delay; comparison with the estimate from eq 6 indicated a closer correspondence between the heterogeneous and target models. However, when the ΔΔOD signals were calculated using the scaling values, the homogeneous model showed a closed resemblance to the corresponding signals calculated by applying the scaling factors found using eq 6. This was true for all excitation wavelengths (λ = 620, 640, 660, and 680 nm) and time delays (d = 1, 14, and 160 ps).

The calculations for the scaling factor discussed are especially important as the wavelengths chosen are resonant with both ground and excited states. Between 640 and 680 nm the PDP/PRP experiment reveals the relative cross sections, and this could be extended to longer wavelengths by using two-color PDP excitation, which employs red-shifted dump or repump wavelengths. Although two-color PDP experiments can be more selective for SE in the dump interaction, the population analysis based on photoselection theory and modeling to extract corrected ΔΔOD signals should still be performed, as excitation away from peak resonance with intense femtosecond visible excitation generally triggers some measurable signal.

Table 3. Photolyzed Fraction Estimates[a]

wavelength (nm)	ΔOD/OD (1)	ΔOD/OD (2)	⟨n⟩ theoretical (1)	⟨n⟩ theoretical (2)	QY (1)	QY (2)
620	7.0%	9.2%	26.5%	18.7%	0.26	0.49
640	8.5%	11.3%	32.1%	22.3%	0.27	0.51
660	8.0%	11.6%	28.2%	20.7%	0.28	0.56
680	3.5%	4.8%	19.2%	14.0%	0.18	0.34

[a] The estimated photolyzed fraction of the sample, caused by the pump (1) and dump/repump (2) excitation pulses in isolation. The fractions are calculated using photoselection theory (⟨n⟩ theoretical) and using the GSB component from spectral fitting of the experimental signal to estimate the photolyzed fraction from eq 7 (ΔOD/OD). QY is the ratio of the experimental (ΔOD/OD) and theoretical photolyzed fraction for each pulse.

Table 4. Scaling Factors for (α) 1 ps Delay[a]

wavelength (nm)	heterogeneous	homogeneous	target	$1-\beta(t)$
620	0.84	0.81	0.82	0.83
640	0.80	0.77	0.77	0.78
660	0.81	0.78	0.79	0.80
680	0.92	0.90	0.91	0.91

[a] Scaling factors, α, for a 1 ps delay between pump and dump/repump for the excitation wavelengths and connectivity schemes as indicated. The scaling factor is to correct for the reduced ground state population the dump/repump pulse interacts with. Values depend on delay between pump and dump/repump pulses and on the connectivity scheme to predict the ground state population. Estimated using eq 6.

Table 5. Scaling Factors (α) for 14 ps Delay[a]

wavelength (nm)	heterogeneous	homogeneous	target	$1-\beta(t)$
620	0.93	0.82	0.95	0.90
640	0.92	0.77	0.94	0.88
660	0.92	0.79	0.94	0.88
680	0.97	0.93	0.98	0.95

[a] Scaling factors, α, for a 14 ps delay between pump and dump/repump for the excitation wavelengths and connectivity schemes as indicated. The scaling factor is to correct for the reduced ground state population the dump/repump pulse interacts with. Values depend on delay between pump and dump/repump pulses and on the connectivity scheme to predict the ground state population. Estimated using eq 6.

Table 6. Scaling Factors (α) for 160 ps Delay[a]

wavelength (nm)	heterogeneous	homogeneous	target	$1-\beta(t)$
620	0.98	0.92	0.98	0.97
640	0.97	0.90	0.98	0.96
660	0.97	0.91	0.98	0.97
680	0.99	0.96	0.99	0.98

[a] Scaling factors, α, for a 160 ps delay between pump and dump/repump for the excitation wavelengths and connectivity schemes as indicated. The scaling factor is to correct for the reduced ground state population the dump/repump pulse interacts with. Values depend on delay between pump and dump/repump pulses and on the connectivity scheme to predict the ground state population. Estimated using eq 6.

Global fitting of the pump−probe measurements using the homogeneous model shows negligible spectral differences between the first ∼2.5 ps and second ∼16 ps components (Figure 3). To experimentally distinguish the underlying population transfer dynamics, PDP and PRP experiments were conducted with 1, 14, and 160 ps delays, which target the three kinetic phases.

The three dump/repump delays (1, 14, and 160 ps) used were to target the three time constants observed in the pump−probe experiments. Whereas all wavelengths are resonant with the ground state, resulting in indistinguishable TA signals that scale with the ground state cross section and power density, dump and repump excitations probed the absorption cross sections of transient and excited states by causing population transfer.

3.6. Pump−Dump/Repump−Probe Transient Absorption Spectroscopy. Even though the ΔΔOD spectral shapes are analogous for a range of scaling factors, it is important to be confident that the scaling factor applied is accurate, as varying α (eq 5) can lead to a sign change in the amplitude of the ΔΔOD signal (eq 2), and in this case the use of an inaccurate scaling factor can make correct interpretation of the data impossible.

The ΔΔOD signals have been calculated using the homogeneous, heterogeneous, and target models by applying the corresponding scaling factors. For all models and time delays (1, 14, and 160 ps) the ΔΔOD signals for excitation at 620, 640, and 660 nm were comparable. Excitation at 680 nm gave distinct spectral features, compared to shorter wavelength excitation, for all models.

The ΔΔOD signals separated the models into two categories with correspondence between the signals calculated using the heterogeneous and target models as well as between the homogeneous model and the signal derived from the results of eq 9. ΔΔOD signals, for the homogeneous and target models (for 640 and 680 nm excitation), are shown in Figures 5 and 6 as they are representative of the differences seen between both excitation wavelength and applied model. ΔΔOD signals for all excitation wavelengths and time delays (for the homogeneous model) are shown in the Supporting Information (Figures S4−6). Once the pump−probe signal has been subtracted from the ΔΔOD signals, there is no amplitude before the arrival of the dump/repump pulse, for all signals, so time zero is chosen to coincide with the dump/repump arrival for all pump−dump delays (1, 14, 160 ps).

With a 160 ps delay, targeting the Lumi-R ground state intermediate, the only resolvable ΔΔOD arose from excitation at 640 and 660 nm. The ΔΔOD signal for this delay (when resolvable) produced signals with spectral shape similar to the 14 ps delay, although with reduced amplitude, for all models.

When applying the scaling factors corresponding to the homogeneous model, the ΔΔOD signals and time traces for 1 and 14 ps dump/repump delay and 620, 640, and 660 nm excitation appear similar to TA spectra presented in this work (Figure 5 a and b). The instantaneous spectrum (Figure 4) includes a GSB feature around 670 nm, SE at longer wavelengths (≈ 700 nm), and an ESA from 500 to 640 nm. These features correspond to an instantaneous decrease in population of a state spectrally similar to the ground state and an increase in excited state. The ΔΔOD

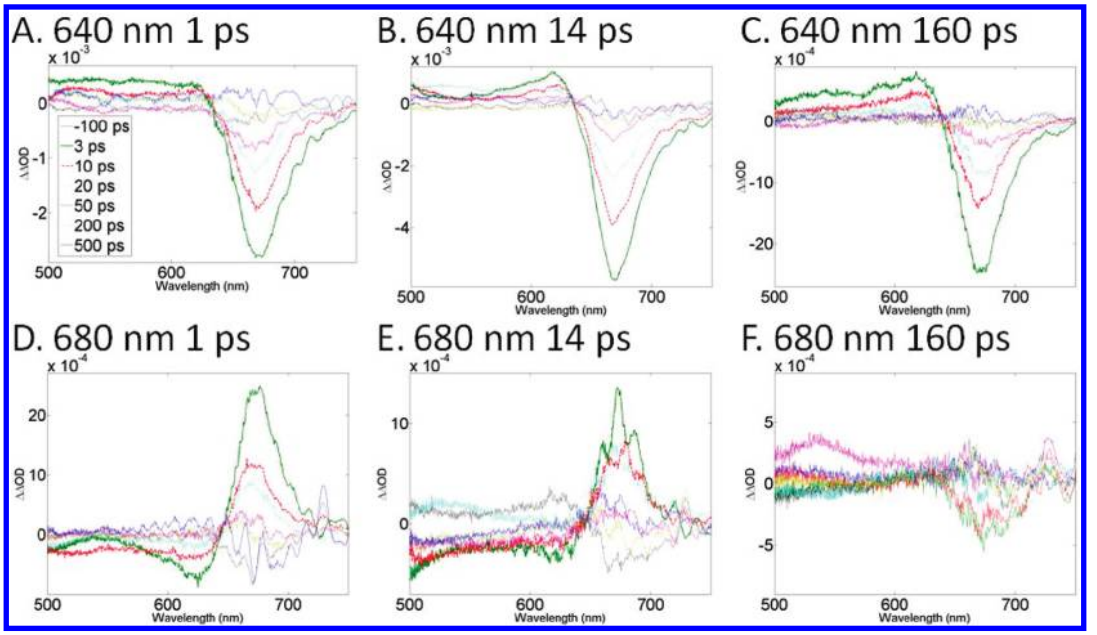

Figure 5. ΔΔOD signals at probe time delays, relative to the dump/repump pulse, as indicated in the legend (with $t = 0$ corresponds to the arrival of the dump/repump), titles indicate excitation wavelength and time delay between the pump and dump/repump pulse. Signals are calculated using the homogeneous model scaling factors (α) for excitation at 640 nm (top row) and 680 nm (bottom row) to show the change in sign of the spectral features for time delays between the pump and dump/repump pulse (1, 14, 160 ps) as indicated.

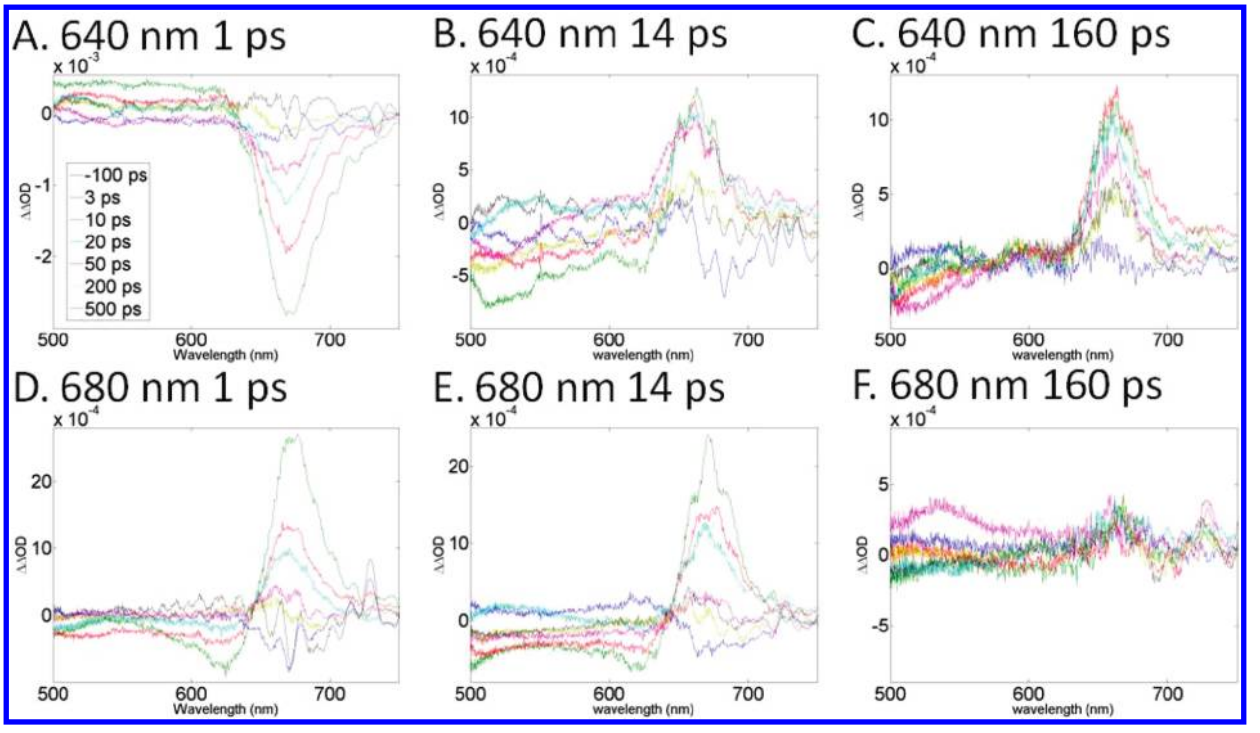

Figure 6. ΔΔOD signals at probe time delays, relative to the dump/repump pulse, as indicated in the legend ($t = 0$ corresponding to the arrival of the dump pulse), titles indicate excitation wavelength and time delay between the pump and dump/repump pulse. Signals are calculated using the target model scaling factors (α) for excitation at 640 nm (top row) and 680 nm (bottom row) to show the change in sign of the spectral features for time delays between the pump and dump/repump pulse (1, 14, 160 ps) as indicated.

signals decayed with picosecond time constants to coincide with amplitude and kinetics of the pump−probe measurements.

In contrast, the target model's ΔΔOD signals showed a sign change between the 1 and 14 ps delay for shorter wavelength excitation (620, 640, 660 nm) which can be seen in Figure 6a and 6b for excitation at 640 nm which is representative of short wavelength excitation. The difference in sign when compared to the corresponding pump−probe spectra (Supporting Information,

dx.doi.org/10.1021/jp206298n |J. Phys. Chem. B 2012, 116, 1077–1088

Table 7. Time Constants from Analysis of the 1 ps ΔΔOD Signal[a]

λ (nm)	τ_1 (ps)	τ_2 (ps)	τ_3 (ps)
620	3.28 ± 0.01	36.08 ± 0.80	long lived
640	2.23 ± 0.01	15.88 ± 0.39	366.21 ± 14.54
660	2.11 ± 0.02	14.26 ± 0.16	497.4 ± 17.28
680	2.27 ± 0.01	18.13 ± 0.41	long lived

[a] Time constants, τ_i, from global analysis of the 1 ps pump−dump/repump delay ΔΔOD data using a homogeneous model. Global analysis was performed on complete, background corrected data sets with excitation at 620, 640, 660, and 680 nm up to 2 ns delay from the pump pulse. The error given is the standard deviation.

Table 8. Time Constants from Analysis of the 14 ps ΔΔOD Signal[a]

λ (nm)	τ_1 (ps)	τ_2 (ps)	τ_3 (ps)
620	2.30 ± 0.16	16.97 ± 0.34	1470 ± 175.7
640	2.36 ± 0.01	16.81 ± 0.01	359.54 ± 11.12
660	2.29 ± 0.01	16.21 ± 0.02	2346.2 ± 257.97
680	2.28 ± 0.01	44.03 ± 2.25	long lived

[a] Time constants, τ_i, from global analysis of the 14 ps pump−dump/repump delay ΔΔOD data using a homogeneous model. Global analysis was performed on complete, background corrected data sets with excitation at 620, 640, 660, and 680 nm up to a 2 ns delay from the pump pulse. The error given is the standard deviation.

Table 9. Time Constants from Analysis of the 160 ps ΔΔOD Signal[a]

λ (nm)	τ_1 (ps)	τ_2 (ps)	τ_3 (ps)
640	2.37 ± 0.01	18.12 ± 0.19	long lived
660	2.34 ± 0.01	15.91 ± 0.26	long lived

[a] Time constants, τ_i, from global analysis of the 160 ps pump−dump/repump delay ΔΔOD data using a homogeneous model. Global analysis was performed on complete, background corrected data sets with excitation at 620, 640, 660, and 680 nm up to a 2 ns delay from the pump pulse. The error given is the standard deviation.

Figure 1) indicates population transfer to the electronics ground state. The instantaneous positive ground state feature implies a different process is dominating at later delay times, for this connectivity scheme.

With all models and delay times, excitation at 680 nm (Figure 5 d and e) produced an instantaneous positive ground state feature indicating population transfer to form the electronic ground state, which is corroborated by the instantaneous negative excited state (ESA) feature from 540 to 640 nm, corresponding to a decrease in excited state population. At long probe times the ΔΔOD signal demonstrates no difference to ΔOD long time signals, as with the measurements at shorter excitation wavelengths.

Due to the correspondence between the signal amplitudes calculated by applying the homogeneous scaling factors and the scaling factors calculated using eq 6, the ΔΔOD signals corresponding to the homogeneous scaling factors were globally fitted. Results of global analysis of the ΔΔOD signal, using a homogeneous scaling factor and connectivity scheme, are summarized in Tables 7−9 for 1, 14, and 160 ps excitation pulse delays, respectively. The related species associated spectra are shown in the Supporting Information (Figures S7−9); two time constants and a long-lived component or three time constants are needed to fit the data successfully.

Analysis of the dump/repump amplitudes, from the homogeneous model, indicates a clear dependence of the transient populations on the different dump/repump times used. For excitation at 620, 640, and 660 nm, the amplitude of the ground state like feature is maximal for the 14 ps delay compared to a 1 or 160 ps delay. Considering the differences in power density used, this is consistent with the presence of a GSI within 1 ps, which increases in population at 14 ps. The amplitude differences between the wavelengths used indicate the cross section of the GSI to be maximal between 640 and 660 nm, similar to that of the Pr ground state. Compared to the Pr ground state, however, the absolute cross section must be smaller for the short-lived GSI to result in the prominent GSB/SE feature in the pump−probe data (Figure 3). Taking the time constants from the ΔΔOD signals imposing a homogeneous model as an indication of the population lifetime of the GSI indicates that primarily the 2.5 ps phase is productive in the formation of the GSI. However, the branching ratios from the 2.5 and 15 ps components to the GSI are not resolved from these experiments; it is possible that the 15 ps component is productive on forming the GSI, if its branching amplitude exceeds that of the 2.5 ps component significantly.

Similar conclusions can be drawn on the GSI cross section from the application of the target (or heterogeneous) model. The sign change seen between the 1 and 14 ps delay times denotes that the GSI is not populated to sufficient levels to resolve it 14 ps after excitation. The reduction in the GSI population at 14 ps, for the target connectivity scheme, implies it is only the 2.5 ps component that is productive in forming GSI. The positive ground state feature that dominates the 14 ps ΔΔOD signal indicates that at this delay SE dominates.

At 160 ps only the transient Lumi-R state is present, which is repumped with 640 and 660 nm excitation to reveal signals that are spectral similar to the 14 ps delay signals for all connectivity schemes.

For excitation at 680 nm the amplitude decreases with increasing decay time as the excited state population decays. This is consistent with population inversion via SE of the S1 population that is linked to both the 2.5 and 15 ps kinetic phases.

4. DISCUSSION AND CONCLUSION

The time constants determined from the analysis of the pump−probe experiment were alike for all excitation wavelengths used. From the spectral and dynamic similarity, it is likely that the same intermediates and decay pathways were created independent of excitation wavelength used (620−680 nm). No indication of thermal cooling processes was resolved with excitation at 620 nm, in contrast to previously reported measurements of the Pr state of Cph1.[13]

The time constants obtained from analysis of the pump−probe experiment are also consistent with those reported in the literature. A visible pump−probe experiment previously carried out on the Pr state of Cph1[13] described the decay of the excited state using a distribution of rate constants centered at 16 ps. The results were also fitted using the sum of two exponentials giving time constants of 12 and 48 ps. Two different excitation wavelengths were employed in the previous pump−probe experiment

(615 and 650 nm), and broadening of the GSB feature was reported at the shorter excitation wavelength. This broadening at shorter wavelengths was not detected in this experiment, although the shortest excitation wavelength used was 620 nm. The dispersive measurements presented here indicate that ultrafast, femtosecond motion in the Franck−Condon region is complete within the instrument response time.

The Pr state of Cph1 has also been studied in the infrared, and the results of ultrafast infrared TA spectroscopy of Cph1[6] indicated that three time constants were needed to fully discribe the decay: 3, 14, and 134 ps. These time constants are very similar to the time constants established from the analysis of the pump−probe data described in this paper (Table 1). The previously reported infrared spectroscopy experiments were modeled by applying a heterogeneous model.[6] In this work a homogeneous and a target model were also used to describe the data with equal success to the heterogeneous model. No conclusion can be drawn on which connectivity scheme is correct from the pump−probe experiments alone.

FSRS measurements of the Pr state of Cph1 reported time constants of 500 fs, 3 ps, and 30 ps.[10] From our TA measurements, with time resolution of 400 fs, there was no indication of a 500 fs component in the decay. However, we note that with a 1 ps dump/repump time a measurable population of a GSI was already present. This GSI population must result from ultrafast internal conversion reactions on similar time scales (Figures 5 and 6). From the FSRS results of Cph1, a connectivity scheme was proposed where the branching between product formation or ground state reformation occurs with a 500 fs time constant. Application of the target connectivity scheme to the PDP/PRP data reported here also supports an early branching point, with the GSI population being diminished at 14 ps compared to 1 ps. PDP/PRP measurements of the Pr state of Cph1 with mid-infrared detection previously reported the presence of a GSI.[15] Specifically, using a 14 ps dump/repump delay, instantaneous decrease of the absorption of a 1608 cm^{-1} band was observed. Induced absorption in this region is characteristic of the C═C stretching mode with an electronic ground state configuration. This was taken as an indication of the presence of a GSI, which was repumped at 14 ps. A GSI has also been inferred in the phytochrome Agp1 from *Agrobacterium* from vis-pump IR-probe and vis-pump vis-probe experiments.[31,32]

Due to the overlapping absorption contributions, detemining GSI electronic absorption features is difficult. It is expected that the GSI absorption maximum would be red-shifted relative to the GSB belonging to the Pr ground state seen in pump−probe signals. This anticipated red shift is not resolved in the ΔΔOD data (Figures 5 and 6), although this could be due to the spectrally overlapping SE and ESA. Particularly, if the Stokes shift for the GSI is smaller than the Stokes shift of the Pr state, a shift in the bleach maximum may not result. The spectral similarity to the electronic Pr ground state seen in the ΔΔOD data for 1 ps delay (which contains no contribution from the interaction of the dump/repump pulse with the ground state) permits the conclusion of the existence of a GSI without a distinct spectral signature which was resolved in the infrared PDP/PRP experiments. The GSI is characterized by reduced cross section relative to the Pr ground state, and the subsequent picosecond dynamics after dumping further supports the assignment to an unrelaxed electronic ground state intermediate. TRIR measurements of the GSI indicated a loss of structure in the C═C stretching region (1611, 1633, and 1653 cm^{-1}), suggesting structural unrelaxed chromophore and environment. In addition, with repumping of GSI at 14 ps, induced absorption in the double difference spectrum at 1570−1580 cm^{-1} was observed that is not present in the Pr spectrum in addition to induced absorption of the C_{19}═O frequency at 1710 cm^{-1} which is also distinct from Pr. The spectrum of the GSI furthermore showed a decreased absorption band at 1654 cm^{-1}, which is close to the 1652 cm^{-1} band in Pr, indicating that the GSI is likely in the C_{15}-Z configuration.[15]

By varying the excitation wavelengths in the pump−probe and PDP/PRP experiments, the relative absorption cross sections can be tracked, which support the inference of the presence of a GSI with a similar, but reduced, absorption cross section to the ground state. We observe a change in relative cross sections of the GSI and SE between 660 and 680 nm, from the change in sign of the instantaneous amplitude in the ΔΔOD data (Figures 5 and 6). Considering the 0−0 transition for the Pr state around 670 nm[30] (Figure 4), this suggests that the GSI absorbs maximally close to the Pr state. Our results presented here are in agreement with the infrared PDP/PRP observations.[15]

The 1 ps delay ΔΔOD signals (and 14 ps delay when applying the homogeneous model) measured in the visible region are also assigned to the repumping of populations with an electronic ground state configuration. The time-resolved measurements of ΔΔOD at 14 ps repump delay are also broadly in agreement, with a dominant 6 ps component. IR detection also reported a 600 ps contribution that was not observed with visible detection (Table 8). Furthermore, scaling factors applied in this work explicitly used the estimated quantum yield, which improved on those previously used,[15] and were discussed in other recent work.[27]

The wavelength dependence of the ΔΔOD signals clearly indicates that at 680 nm stimulated emission proceses dominated. SE processes dominate the 680 nm ΔΔOD signals for all models and time delays applied to the data. A change in the sign of instantaneous absorption for the dump/repump excitation at 1 ps occurred from 660 to 680 nm for all connectivity schemes (Figures 5 and 6). This signifies an increased stimulated emission cross section at this wavelength. This agrees with the fluorescence spectrum with a maximum at λ = 680 nm (Figure 4). These results clearly indicate that both the 2.5 and 15 ps components include S1 decay reactions, corroborated by the presence of SE from λ = 660 to 700 nm in the species associated difference spectra from the homogeneous model applied to the ΔOD pump−probe measurements (Figure 3).[9,13,33,34]

The GSI is resolved with all models applied for the 1 ps delay, but differences are seen between the models for the 14 ps delay. This is due to the variations in the population estimates between the different models being greatest for this delay.

For the homogeneous decay pathway, the amplitude of the ground state feature for the 1 ps delay between the two excitation pulses is less than for a 14 ps delay; this suggests that the population of the GSI is larger at 14 ps than at 1 ps after the creation of the excited state. By judging the relative amplitudes assigned to repumping of the GSI at 1 and 14 ps, considering the power densities used, this suggests that primarily the 2.5 ps component is productive, assuming the homogeneous decay pathway to be correct.

When the target model is imposed the amplitude of the ground state feature in the ΔΔOD signal changes sign between the 1 and 14 ps delay times. This suggests that the population of the GSI has decreased between 1 and 14 ps after excitation so that at 14 ps SE processes dominate and the GSI is not resolved. This change in amplitude suggests that the 2.5 ps component could be the only productive component in populating the GSI.

The detection of the GSI using multipulse spectroscopy allows the conclusion that the target model shown in Figure 1 most accurately represents the connectivity scheme in the phytochrome Cph1. The conclusion is in agreement to the previously reported results of infrared multipulse spectroscopy of Cph1.[15] The GSI forms part of the decay back to the ground state when the absorbed light has not lead to successful photoisomerization. Since it reports on the unproductive pathway, it provides information that is relevant to the relatively low quantum yield of photoisomerization.

With repumping the Lumi-R ground state intermediate at 160 ps, that is formed with ~10% quantum yield, ΔΔOD signals are observed that may be assigned to Lumi-R* or the S1 state of the C15-E configuration of the phycocyanobilin chromophore. The scaling factor α, at 160 ps, under the conditions used approaches unity, and therefore errors should be very minor, although differences are seen between the applied connectivity schemes. The spectral differences indicate that Lumi-R* absorbance strongly overlaps with Pr−S1. This further illustrates that global analysis of pump−probe difference spectra yields spectral differences that contain contributions from several excited and ground state intermediates, all with different cross sections, population decay characteristics, and connectivities.

Here, multipulse control spectroscopy has helped to disentangle spectral and kinetic features of these populations in a semi-quantitative manner. By tracking the time-dependent cross section and population transfers, we have been able to resolve a GSI and demonstrate an increase in the SE cross section from the S1 state at longer excitation wavelengths. We additionally show that a systematic approach to characterize photolysis and population dynamics from experimental parameters is essential to the analysis of multipulse control spectroscopy.[27]

■ ASSOCIATED CONTENT

Supporting Information. Pump−probe spectra for various time delays are shown in Figure S1; S2 and S3 show species associated difference spectra for pump−probe data fitted with the target and heterogeneous models. S4−6 display ΔΔOD signals for various time points for all excitation wavelengths and 1, 14, and 160 ps pump−dump/repump delays. Homogenously fitted species associated difference spectra for ΔΔOD data are shown in Figures S7−9 for pump−dump/repump delays of 1, 14, and 160 ps. The results of global fitting the pump−probe data using heterogeneous and target models are shown in Tables S1 and S2. This material is available free of charge via the Internet at http://pubs.acs.org.

■ AUTHOR INFORMATION

Corresponding Author
*E-mail: j.vanthor@imperial.ac.uk.

■ ACKNOWLEDGMENT

We thank Mr. B. Kellner and Dr. K.C. Toh for assistance with sample preparation. JJvT acknowledges support from the European Research Council via grant agreement No. 208650 and from the Royal Society.

■ REFERENCES

(1) Rockwell, N. C.; Lagarias, J. C. *ChemPhysChem* **2010**, *11*, 1172.
(2) Lamparter, T. *FEBS Lett.* **2004**, *573*, 1.
(3) Montgomery, B. L.; Lagarias, J. C. *Trends Plant Sci.* **2002**, *7*, 357.
(4) Rockwell, N. C.; Su, Y.-S.; Lagarias, J. C. *Annu. Rev. Plant Biol.* **2006**, *57*, 837.
(5) Ulijasz, A. T.; Cornilescu, G.; von Stetten, D.; Kaminski, S.; Mroginski, M. A.; Zhang, J.; Bhaya, D.; Hildebrandt, P.; Vierstra, R. D. *J. Biol. Chem.* **2008**, *283*, 21251.
(6) van Thor, J. J.; Ronayne, K. L.; Towrie, M. *J. Am. Chem. Soc.* **2007**, *129*, 126.
(7) van Thor, J. J.; Borucki, B.; Crielaard, W.; Otto, H.; Lamparter, T.; Hughes, J.; Hellingwerf, K. J.; Heyn, M. P. *Biochemistry* **2001**, *40*, 11460.
(8) van Thor, J. J.; Mackeen, M.; Kuprov, I.; Dwek, R. A.; Wormald, M. R. *Biophys. J.* **2006**, *91*, 1811.
(9) Andel, F.; Hasson, K. C.; Gai, F.; Anfinrud, P. A.; Mathies, R. A. *Biospectroscopy* **1997**, *3*, 421.
(10) Dasgupta, J.; Frontiera, R. R.; Taylor, K. C.; Lagarias, J. C.; Mathies, R. A. *Proc. Natl. Acad. Sci. U.S.A.* **2009**, *106*, 1784.
(11) Fischer, A. J.; Lagarias, J. C. *Proc. Natl. Acad. Sci. U.S.A.* **2004**, *101*, 17334.
(12) Foerstendorf, H.; Lamparter, T.; Hughes, J.; Gärtner, W.; Siebert, F. *Photochem. Photobiol.* **2000**, *71*, 655.
(13) Heyne, K.; Herbst, J.; Stehlik, D.; Esteban, B.; Lamparter, T.; Hughes, J.; Diller, R. *Biophys. J.* **2002**, *82*, 1004.
(14) van Thor, J. J.; Fisher, N.; Rich, P. R. *J. Phys. Chem. B* **2005**, *109*, 20597.
(15) van Wilderen, L. J. G. W.; Clark, I. P.; Towrie, M.; van Thor, J. J. *J. Phys. Chem. B* **2009**, *113*, 16354.
(16) Gai, F.; McDonald, J. C.; Anfinrud, P. A. *J. Am. Chem. Soc.* **1997**, *119*, 6201.
(17) Kennis, J. T. M.; Larsen, D. S.; van Stokkum, I. H. M.; Vengris, M.; van Thor, J. J.; van Grondelle, R. *Proc. Natl. Acad. Sci. U.S.A.* **2004**, *101*, 17988.
(18) Larsen, D. S.; Papagiannakis, E.; van Stokkum, I. H. M.; Vengris, M.; Kennis, J. T. M.; van Grondelle, R. *Chem. Phys. Lett.* **2003**, *381*, 733.
(19) Larsen, D. S.; van Stokkum, I. H. M.; Vengris, M.; van der Horst, M. A.; de Weerd, F. L.; Hellingwerf, K. J.; van Grondelle, R. *Biophys. J.* **2004**, *87*, 1858.
(20) Larsen, D. S.; Vengris, M.; van Stokkum, I. H. M.; van der Horst, M. A.; de Weerd, F. L.; Hellingwerf, K. J.; van Grondelle, R. *Biophys. J.* **2004**, *86*, 2538.
(21) Logunov, S. L.; Volkov, V. V.; Braun, M.; El-Sayed, M. A. *Proc. Natl. Acad. Sci. U.S.A.* **2001**, *98*, 8475.
(22) Papagiannakis, E.; Vengris, M.; Larsen, D. S.; van Stokkum, I. H. M.; Hiller, R. G.; van Grondelle, R. *J. Phys. Chem. B* **2006**, *110*, 512.
(23) Rupenyan, A.; van Stokkum, I. H. M.; Arents, J. C.; van Grondelle, R.; Hellingwerf, K. J.; Groot, M. L. *J. Phys. Chem. B* **2009**, *113*, 16251.
(24) Wohlleben, W.; Buckup, T.; Hashimoto, H.; Cogdell, R. J.; Herek, J. L.; Motzkus, M. *J. Phys. Chem. B* **2004**, *108*, 3320.
(25) Mukamel, S. *Principles of nonlinear optical spectroscopy*; Oxford University Press: New York, 1995.
(26) van Thor, J. J.; Zanetti, G.; Ronayne, K. L.; Towrie, M. *J. Phys. Chem. B* **2005**, *109*, 16099.
(27) van Wilderen, L. J. G. W.; Lincoln, C. N.; van Thor, J. J. *PLoS ONE* **2011**, *6*, e17373.
(28) Ansari, A.; Szabo, A. *Biophys. J.* **1993**, *64*, 838.
(29) van Stokkum, I. H. M.; Larsen, D. S.; van Grondelle, R. *Biochim. Biophys. Acta* **2004**, *1657*, 82.
(30) Sineshchekov, V.; Hughes, J.; Hartmann, E.; Lamparter, T. *Photochem. Photobiol.* **1998**, *67*, 263.
(31) Schumann, C.; Groß, R.; Michael, N.; Lamparter, T.; Diller, R. *ChemPhysChem* **2007**, *8*, 1657.
(32) Schumann, C.; Groß, R.; Wolf, M. M. N.; Diller, R.; Michael, N.; Lamparter, T. *Biophys. J.* **2008**, *94*, 3189.
(33) Brock, H.; Ruzsicska, B. P.; Arai, T.; Schlamann, W.; Holzwarth, A. R.; Braslavsky, S. E.; Schaffner, K. *Biochemistry* **1987**, *26*, 1412.
(34) Teuchner, K.; Schulz-Evers, M.; Leupold, D.; Strehlow, D.; Rüdiger, W. *Chem. Phys. Lett.* **1997**, *268*, 157.